Molecular Simulations on the Coalescence of Water-in-Oil Emulsion Droplets with Non-ionic Surfactant and Model Asphaltene

Xiaoyu Sun[†], *Hongbo Zeng*[*,†], *Tian Tang*[*,‡]

[†]*Department of Chemical and Materials Engineering, University of Alberta, Edmonton, AB T6G 1H9, Canada*

[‡]*Department of Mechanical Engineering, University of Alberta, Edmonton, AB T6G 1H9, Canada*

** Corresponding authors:*

E-mail: hongbo.zeng@ualberta.ca (H.Z.); Phone: +1-780-492-1044;

E-mail: tian.tang@ualberta.ca (T.T.); Phone: +1-780-492-5467.

ABSTRACT

Water droplets in crude oil can be stabilized by the adsorption of interfacially active components, such as asphaltenes. Demulsifiers like non-ionic surfactants are commonly used to destabilize the water-in-oil emulsions. In this work, molecular dynamics simulations and free energy calculations were performed to study the coalescence of water droplets coated with both model asphaltene and non-ionic surfactants (PEO-PPO-PEO copolymer (SurP) or Brij surfactant (SurB)). For the first time, we quantitatively studied the interaction force between water droplets with the presence of both asphaltenes and demulsifiers, and addressed the effect of solvent property on the coalescence process. At the droplet surface, demulsifiers adsorbed closer to the water phase and formed more hydrogen bonds with water molecules compared to asphaltenes, indicating the capability of demulsifiers to break the asphaltene film. Comparing the two non-ionic surfactants, VO-79/SurP complexes formed a single-layer film on the droplet surface, while a two-layer structure was formed by VO-79/SurB complexes. This led to a higher repulsive force during droplet coalescence when SurB was present, regardless of the type of solvent. Comparing the two different solvents (toluene vs. heptane), for the same adsorbates the interfacial film was more compact in heptane and there were fewer dispersed VO-79. For VO-79/SurB adsorbates, this led to smaller repulsion during droplet coalescence when the solvent was heptane, while the difference is insignificant for VO-79/SurP adsorbates. This work suggests that the energy barrier and interaction force for droplet coalescence is highly dependent on the structure of interfacial films, thus providing atomic-level insights into the demulsification mechanisms of water-in-oil emulsions in the presence of surface-active asphaltenes.

1. Introduction

Droplet coalescence exists in many natural and industrial processes, such as the formation of rain drops[1], spray drying[2,3], emulsification and demulsification[4]. Water and oil are immiscible, however, water droplets dispersed in the oil phase could be stabilized by the interfacially-active components, e.g. asphaltene.[5–7] In fact, asphaltene is the heaviest and most polar group in crude oil, and a main contributor to stable water-in-oil (W/O) emulsions.[8] Such emulsions are highly undesirable in the petroleum industry as they could cause severe fouling and corrosion problems in the downstream operations.[7,9] Stability of W/O emulsions is dependent on many conditions, including solvent types or composition of the oil phase[4,10], temperature[11–13], ionic strength[14–16], and the presence of demulsifiers[17,18]. Various demulsification methods have been applied to destabilize water droplets in the oil phase.[19–23] Understanding droplet coalescence is of fundamental importance for uncovering the mechanisms of emulsification and demulsification.

Investigations on droplet coalescence started at the end of the 19th century.[24] Since then, the morphologies during droplet coalescence have been studied experimentally and theoretically.[25] For example, high-speed imaging was used to capture the bridging morphologies of two water droplets and illustrate its hydrodynamics under the influence of different viscosity. Chen et al.[26] combined high-speed imaging and numerical simulation to investigate the morphologies of droplet coalescence during the pinch-off process. Perumanath et al.[27] used molecular dynamics (MD) to simulate water droplet coalescence and observed single and multiple bridges initiated by thermal motion.

With the assistance of atomic force microscopy (AFM) and surface force apparatus (SFA), researchers performed experiments to measure the interaction force between droplets during their coalescence.[24] Dagastine et al.[28] explored the feasibility of using AFM to measure the force

between two oil droplets in the aqueous phase. The results were qualitative, but accompanied by numerical modeling that predicted the force as a function of displacement.[28] Carnie et al.[29] developed the first model that took into account several factors, e.g. surface force, hydrodynamics, drop deformation and cantilever deflection, that influenced interaction force between droplets with size of 10-100 μm. Shi et al.[4] used drop probe AFM to investigate the interaction force between W/O emulsion droplets with the presence of asphaltenes. The water droplets were reported to be stabilized by the adsorbed asphaltenes due to steric hindrance.[4] Interfacial behaviors of the asphaltenes and the stability of W/O emulsion droplets were affected by many factors, including asphaltene concentration and solvent types, e.g., toluene, heptane and their mixture at different ratios.[4] In toluene and when asphaltenes were present, there was a repulsive force during the approaching stage and adhesion during separation.[4] In pure heptane, asphaltenes was insoluble and had higher tendency to aggregate, which resulted in adhesion between the interfacial asphaltene films on different water droplets.[4] The corresponding AFM result showed a sudden "jump-in" behavior and the water droplets readily coalesced, indicating that a poor solvent (heptane) could promote the destabilization of water droplets.[4]

In recent years, MD simulations have been performed to provide atomic-level investigations and to quantitatively probe the interaction force between water droplets. Pak et al. simulated bare water droplets[1] and carboxylic acids coated droplets[30] in vacuum, and found that their interaction force was attractive in both cases. They concluded that the collision speed was correlated to the formation of H-bonds between the two water droplets, and was reduced by the presence of coatings.[1,30] By combining MD and AFM, our previous work investigated water droplets in toluene with the presence of a model asphaltene or non-ionic surfactants commonly used as demulsifiers.[31] MD simulations and AFM measurements agreed in that the adsorbate imposed repulsion between

the water droplets.[31] Lower repulsion was observed for adsorbates with higher mobility on the surface during droplet coalescence.[31] One limitation of this work is that only a single component of adsorbates were introduced into the systems, while it is commonly hypothesized that the demulsifiers can penetrate into and break up the asphaltene film at the water/oil interface, leading to the destabilization of W/O emulsions. Understanding the interactions between W/O emulsion droplets with the co-adsorption of model asphaltenes and demulsifiers is necessary in order to uncover the demulsification mechanisms.

In this work, MD simulations were performed on W/O emulsion droplets with the presence of both model asphaltenes and demulsifiers. Free energy and interaction force during droplet coalescence were calculated. Recognizing that the solvent type can have significant impact on the stability of W/O emulsions, this effect was investigated and compared with previous experimental studies. Through quantitative analysis, this work aims to provide insights into the demulsification mechanisms under the mutual influence of asphaltene adsorption, presence of non-ionic surfactants, and solvent properties.

2. Methods.

2.1 Molecular models and simulated systems.

The model asphaltene was represented by a polycyclic aromatic compound (PAC), violenthrane-79 (VO-79, $C_{50}H_{48}O_4$, molecular weight MW: 712 g/mol), as shown in Fig. 1a. While it is primarily used as an organic semiconductor, VO-79 has also been extensively adopted as a model asphaltene due to its structural similarities with the continental-type asphaltenes.[16,32–34] Two non-ionic surfactants were modeled, which have been frequently used as demulsifiers owing to their advantages of low cost and high efficiency.[22,35] With hydrophilic poly(ethylene oxide) (PEO)

and hydrophobic poly(ethylene oxide) (PPO) branches, PEO-PPO-PEO triblock copolymer is a family of polymeric surfactants that has been commonly used as breakers of water-in-oil emulsions.[36] PEO-PPO-PEO copolymers have different structural characteristics, such as hydrophilic-lipophilic balance (HLB), EO/PO ratio, structural isomers etc., which affect their demulsification performance.[35] As shown in Fig. 1a, a model PEO-PPO-PEO copolymer ($PEO_5PPO_{10}PEO_5$, MW: 1039 g/mol) was built and applied as a polymeric demulsifier, which will be referred to as "SurP". It captured the triblock feature of PEO-PPO-PEO copolymer that has two hydrophilic tails and a hydrophobic center. The chain length was scaled down to meet the capability of molecular simulations. Based on the method introduced by Guo et. al.[37], the HLB of SurP was estimated to be 18.9, indicating a high hydrophilicity. Another model non-ionic surfactant, polyethylene glycol octadecyl ether ($C_{22}H_{46}O_3$, MW: 358 g/mol), shares the structural features of Brij surfactants with hydrophilic EO groups and hydrophobic hydrocarbon groups. With its chemical structure shown in Fig. 1a, this molecule will be referred to as "SurB". SurB is an analogy of the surfactant Brij-93, which was shown by Pradilla et al. to be able to replace crude oil-extracted asphaltenes at water/xylene (oil) interface, hence having the potential to destabilize water-in-oil emulsions.[38,39] Compared with SurP, SurB has a shorter chain, a hydrophilic-hydrophobic (instead of hydrophilic-hydrophobic-hydrophilic) structure, and overall higher hydrophobicity.

Force field parameters of the model asphaltene and demulsifiers were developed and validated in our previous work [40–42], where their simulated densities were compared with real materials that they represent. Briefly, the geometry of the non-ionic surfactants was optimized by Gaussian 16 [43] at the B3LYP [44]/6-31G + (d,p) level. Their topologies were then generated by using Automated Topology Builder (ATB)[45]. The partial atomic charges were calculated by CHELPG (CHarges

from ELectrostatic Potentials using a Grid based method)[46], and manually applied to the topologies. The values of the partial atomic charges are given in Supporting Information (SI) section SI1. Simple-point-charge[47] model was used for water molecules. Force field parameters for toluene and heptane were also verified previously[40,48] and used as is.

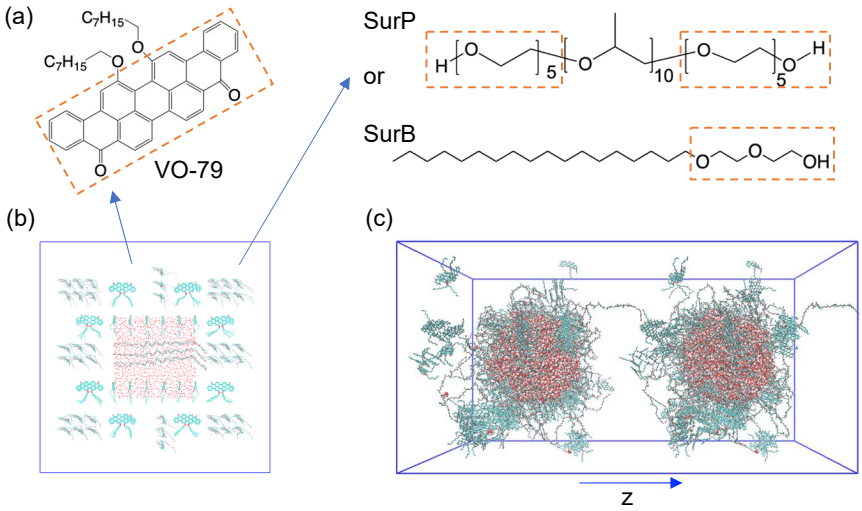

Figure 1. (a) Molecular structures of VO-79 and non-ionic surfactants. For each molecule, the atoms in the orange box(es) are defined as the hydrophilic group and the rest considered as the lipophilic group. Initial configuration for (b) the simulation of a single water droplet (phase 1) and (c) the SMD simulation (phase 2). Water molecules are shown as red (oxygen) and white (hydrogen) spheres; adsorbates are shown in cyan (carbon) and red (oxygen); organic solvents are removed for clarity. Snapshots in (b) and (c) are for sys. Tol-VP.

As shown in Table 1, two sets of systems were simulated, and the systems in each set had the same organic phase, toluene or heptane, indicated in the system names before "-". The first set contained two systems with toluene being the organic phase, Tol-VP and Tol-VB, where "V" stood for VO-79, "P" for SurP and "B" for SurB. In the second set, systems Hep-VP and Hep-VB had heptane as the organic phase. These four systems contained the same number of VO-79 molecules,

Tol-VP and Hep-VP had the same number of SurP, similarly Tol-VB and Hep-VB had the same number of SurB. The number of molecules in each system and the corresponding mass concentrations of the adsorbates are given in Table 1. The systems with two types of adsorbates were accompanied by two reference systems serving as control (Table 1). Tol-V contained 196 VO-79 molecules (10.0 wt.%) in toluene, which was simulated in a previous work[31]. Hep-V also had VO-79 as the only adsorbates, with a similar VO-79 concentration (9.9 wt%).

Table 1. System details. (Numbers are for a single water droplet in each system.)

Sys.	VO-79	SurP	SurB	Water	Toluene	Heptane	Adsorbate Concentration (wt.%)
Tol-VP	104	102	-	4074	12125	-	5.7 (VO-79) + 8.2 (SurP)
Tol-VB	104	-	311	4074	12073	-	5.7 (VO-79) + 8.6 (SurB)
Hep-VP	104	102	-	4074	-	11714	5.5 (VO-79) + 7.8 (SurP)
Hep-VB	104	-	311	4074	-	11437	5.6 (VO-79) +8.4 (SurB)
Control	VO-79	SurP	SurB	Water	Toluene	Heptane	Adsorbate Concentration (wt.%)
Tol-V[31]	196	-	-	4074	13460	-	10.0 (VO-79)
Hep-V	196	-	-	4074		12724	9.9 (VO-79)
Abbreviations: Tol – Toluene; Hep – Heptane; V – VO-79; P – SurP; B – SurB.							

2.2 Simulation details.

MD simulations were performed using the GROMACS software package (version 5.0.7) [49–51] with GROMOS force field parameter set 54A7[52]. To obtain the free energy for water droplet coalescence, the simulation of each system followed a three-phase procedure: (1) equilibration of a single water droplet; (2) coalescence of two water droplets simulated via steered molecular dynamic (SMD); and (3) potential of mean force (PMF) calculation using umbrella sampling (US) simulations.

The initial configuration for phase 1 simulation is shown in Fig. 1b using sys. Tol-VP as an example. The adsorbates were placed on the 6 sides of a cubic water box (5×5×5 nm^3), which contained 4074 water molecules. Organic solvent, toluene or heptane, was then added to the simulations box with a dimension of 14×14×14 nm^3. Each system went through an energy

minimization using the steepest descent method, followed by an NVT equilibration for 100 ps with position-restraints on non-hydrogen atoms. Production run was then carried out in NPT ensemble for 60 ns at 300 K and 1 bar. Parrinello-Rahman[53] barostat with a time constant (τ_p) of 1.0 ps was used for maintaining the pressure. Temperature coupling was achieved by using velocity rescaling thermostat with a time constant (τ_T) of 0.1 ps. LINCS[54] algorithm was used to constrain the intramolecular bonds. Cut-off distance for van der Waals interaction and short-range electrostatics was 1.4 nm, while the smooth Particle-mesh Ewald method was used for long-range electrostatics.[55] Periodic boundary conditions were applied in x, y, and z directions. All simulations had a time step of 2 fs. After equilibration, the final configuration of phase 1 contained a spherical water droplet approximately 6.16 nm in diameter. This configuration was duplicated in z-direction to generate a two-droplet system with a total dimension of $14\times14\times28$ nm^3. The initial separation between the centers of mass (COMs) of the two droplets was half of the simulations box, i.e., 14 nm, which was greater than twice the diameter of the droplets. The two-droplet system served as the initial configuration for phase 2 simulation, as shown in Fig. 1c for sys. Tol-VP.

Phase 2 simulation was SMD for the coalescence of two identical water droplets with coated adsorbates in the organic solvent. Each droplet was defined as a cluster of water molecules where any molecule was within 0.35 nm of at least another molecule in the initial configuration.[56] Two pulling groups were then defined: the droplet on the left (drop1) and the one on the right (drop2). The reaction coordinate (ζ) was chosen to be the separation between the COMs of the two pulling groups. Following energy minimization and NVT equilibration similar to phase 1, SMD was performed where the COMs of the two water droplets were each attached to a spring with force constant of 1000 kJ/(mol·nm^2) and pulled along the head-on direction. To determine a suitable pulling speed, we consulted the SMD simulations of Lemkul et al.[56], where a pull rate of 0.01

nm/ps was shown not to give artifacts compared with lower pull rates (0.005 nm/ps or 0.001 nm/ps). Thus, in this work 0.01 nm/ps was applied on the reaction coordinate ζ, i.e., ζ decreased from its initial value at a constant rate of 0.01 nm/ps (confirmed in SI section SI2). Simulation parameters for SMD were the same as those in the production run of phase 1, except that NVT ensemble was used in SMD. The total pull time was 1.4 ns.

PMF calculation was performed during phase 3 simulation. A set of configurations generated from SMD were selected as the initial configurations for US simulations. The largest value for ζ was the COM separation in the initial configuration of the SMD simulation (~14 nm), and the smallest ζ was the COM separation a few frames after the two droplets merged. In each US window, the system underwent a brief NVT equilibration followed by US simulation, which was performed using the same strategy as in phase 2, except that the spring constant was 2000 kJ/(mol·nm^2) and the pull rate was zero. A good overlap between the histograms from US[57] was achieved, as shown in SI section SI3. Weighted histogram analysis method (WHAM)[58] was used to generate the unbiased PMF as a function of ζ.

3. Results and Discussion

3.1 Co-adsorption of VO-79 and non-ionic surfactant

Data from the last 5 ns of phase 1 simulations were used to calculate the radial distribution functions (RDFs) of the atoms in the adsorbates with respect to the COM of water droplet, as shown in Fig. 2a-2d. Each type of adsorbates had a hydrophilic group (HP) and a lipophilic group (LP), as defined in Fig. 1a. RDFs for the atoms in HP and LP are shown as separate curves in Fig. 2a-2d. The results for the control sys. Tol-V can be found in the previous work[31] and those for sys. Hep-V are shown in SI section SI4. Table S4 in SI section SI4 also summarizes the location and

width of the first and most prominent peak in the RDF curves. In sys. Tol-VP (Fig. 2a), the peak for HP in VO-79 was located at a smaller distance (3.78 nm) than that for LP in VO-79 (4.16 nm), and the peak for all the VO-79 atoms was at 3.88 nm. The curve for all the SurP atoms had a broad distribution and a peak at 3.68 nm, smaller than all three VO-79 peaks. This closer location was caused by the distribution of HP atoms in the SurP, which was narrow with a sharp peak located at 3.30 nm. In contrast, atoms in LP of the SurP were distributed at the outer layer of the interfacial film with its peak location (4.12 nm) similar to that of LP in VO-79. In sys. Tol-VB (Fig. 2b), RDF curves for all atoms, HP and LP of VO-79 were broad and overlapping, located at a large distance (5.26 nm) with low intensity. This indicates that VO-79 molecules were distributed in the outer layer of the interfacial film, and there was no preference for the HP or LP parts of VO-79 to approach water. In comparison, SurB was located at a much closer distance to the water droplet, with the first HP, LP and all atom peaks located at 3.24, 3.76 and 3.54 nm respectively. HP still had more tendency to interact with water, but the preference was smaller than what was observed for the two groups in the SurP. Interestingly, the curve for HP in SurB had another, lower, peak at 4.9 nm, which suggests a two-layer structure formed by SurB near the droplet surface, a first layer in direct contact with water and a second layer consisting of excess SurB molecules attached to the first layer. VO-79 was expelled to the outside of the second SurB layer, forming the most distant part of the interfacial film.

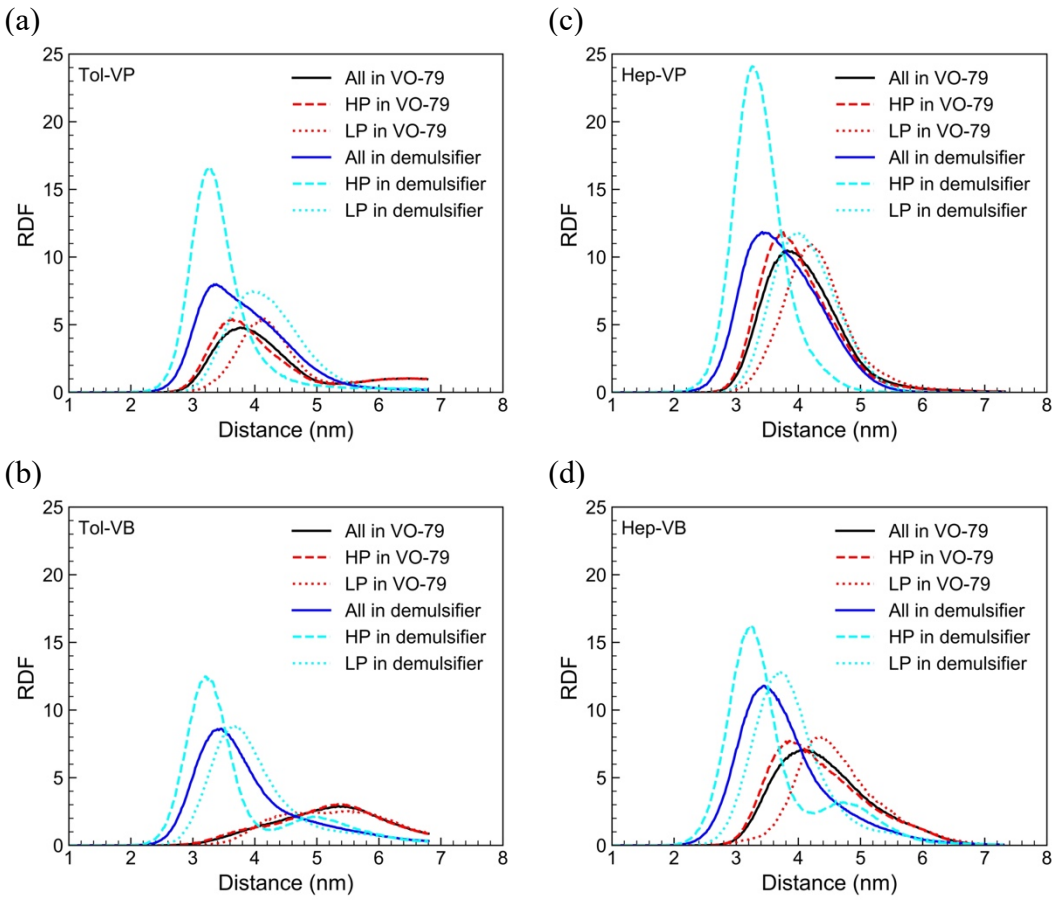

Figure 2. RDF of all atoms, atoms in hydrophilic (HP) and lipophilic (LP) groups of the adsorbates around the COM of the water droplet in phase 1 simulations; data for (a) sys. Tol-VP, (b) sys. Tol-VB, (c) sys. Hep-VP and (d) sys. Hep-VB.

VO-79 is less soluble in heptane and hence has higher tendency to adsorb at the water/heptane interface. This is supported by the comparison between the two control systems Tol-V and Hep-V (SI section SI4): in Hep-V the RDF peaks were closer to water and had smaller width. In accordance with this, the RDF curves for SurP also had higher intensity (Fig. 2c vs. Fig. 2a) and smaller width (SI section SI4) in sys. Hep-VP than in sys. Tol-VP. In both systems, the interfacial film consisted of SurP/VO-79 complexes due to the co-adsorption of both adsorbates, and the higher tendency for VO-79 to adsorb at water/heptane interface might have made the film more

compressed in sys. Hep-VP, as reflected by the narrower RDF peaks. In sys. Hep-VB (Fig. 2d), SurB also formed a two-layer structure, while VO-79 were distributed at a smaller distance to the water droplet compared with sys. Tol-VB (Fig. 2d vs. Fig. 2b, and data from SI section SI4). In fact, the VO-79 peak was between the two peaks for HP in SurB, suggesting strong complexation between VO-79 and SurB. For both sys. Hep-VP and sys. Hep-VB, the atoms from HP of VO-79 and the non-ionic surfactants were in closer contact with water than their counterparts in LP.

Fig. 2a-2d shows that for all four systems, water had stronger interaction with the non-ionic surfactant than with VO-79. This can also be observed directly from snapshots taken during the SMD (phase 2) simulations. Fig. 3a-3d shows the initial configurations (top panel) and the configurations at 0.6 ns (middle panel) and 0.9 ns (bottom panel) of the SMD. The configurations for the control sys. Tol-V and sys. Hep-V are shown in SI section SI5. To distinguish different components, the non-ionic surfactants are shown in blue and the atoms in VO-79 are shown in cyan and red. In Fig. 3a (top panel), SurP molecules adsorbed at the surface of water droplets, with the VO-79 molecules attached to the outside of the SurP layer or dispersed in the organic phase. As the droplets were pulled closer, in Fig. 3a (middle panel), the loosely structured interfacial film redistributed on the droplet surfaces, leaving some areas uncovered. At the onset of coalescence, in Fig. 3a (bottom panel), some of the adsorbate molecules were detached from the interfacial film and dispersed into toluene, which is a "good" solvent for VO-79. Similar phenomenon was observed from the configurations in Fig. 3b where SurB replaced SurP. Upon coalescence (Fig. 3b, bottom panel), the dispersed molecules were almost entirely VO-79, and SurB redistributed at the surface without desorbing into the organic phase. In sys. Hep-VP (Fig. 3c) and sys. Hep-VB (Fig. 3d), the adsorbate films appeared to be thinner and more condensed than their counterparts in sys. Tol-VP and sys. Tol-VB. In the bottom panel of Fig. 3c and Fig. 3d, the adsorbates stayed

on the droplet surfaces when the coalescence was about to occur. Comparing sys. Hep-VP to sys. Tol-VP and sys. Hep-VB to sys. Tol-VB, the surface redistribution of adsorbate molecules was less evident during the approaching of the water droplets in heptane.

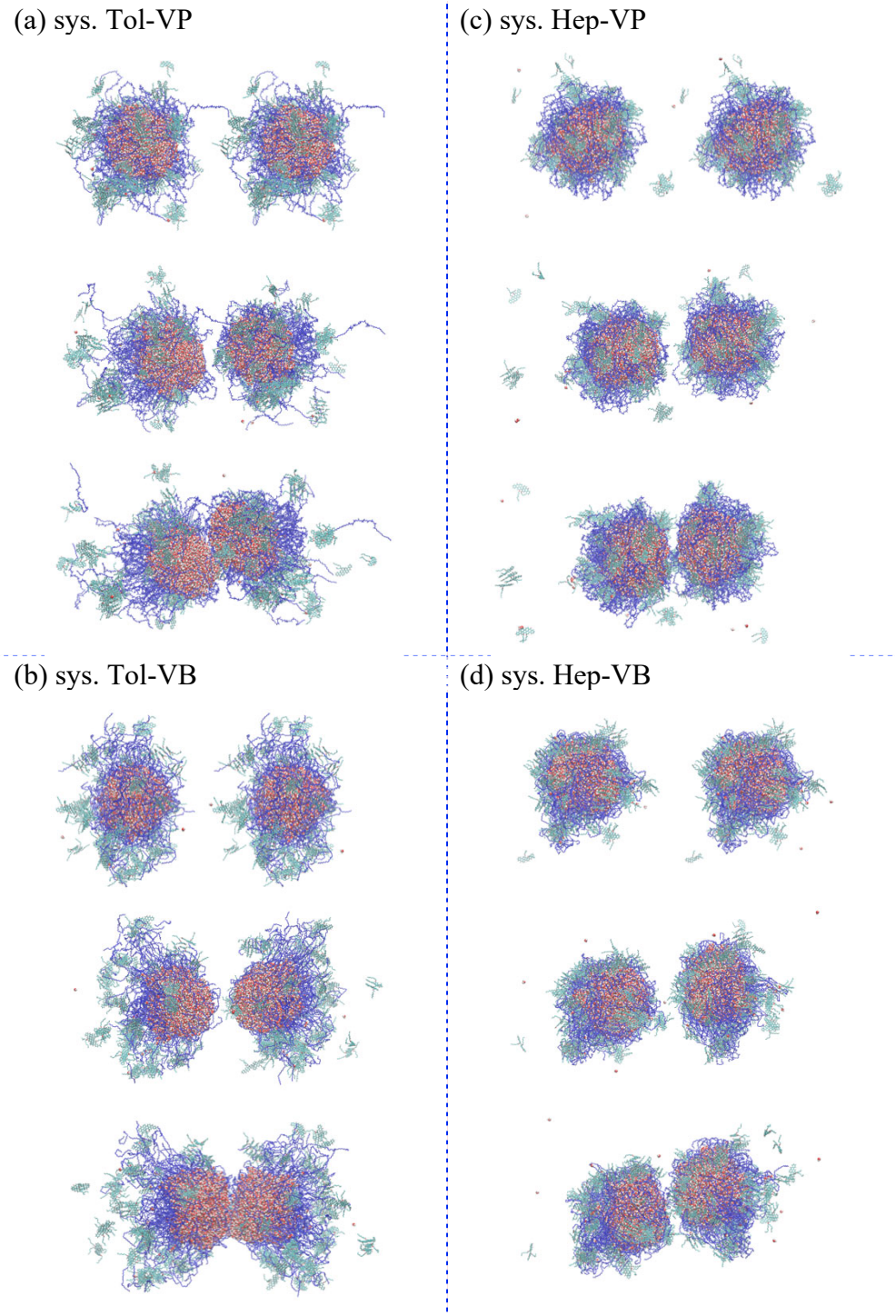

Figure 3. Configurations at 0 (top), 0.6 (middle) and 0.9 (bottom) ns during SMD for (a) sys. Tol-VP, (b) sys. Tol-VB, (c) sys. Hep-VP and (d) sys. Hep-VB. (Red and white spheres: oxygen and hydrogen in water molecules; blue: SurP or SurB; cyan and red connected with bonds: carbon and oxygen in VO-79.)

3.2 Droplets interaction and evolution of molecular contact during coalescence

During SMD (phase 2 simulation), the water droplets were pulled together along the reaction coordinate (ζ, COM separation of two droplets), representing the process of coalescence. The coalescence was under the influence of complex interactions involving different components: water, VO-79, demulsifiers, and organic solvents. In this section, the interactions among different components and evolution of their contacts were examined through the analysis of hydrogen bonding (H-bonding) and aggregation. All results were plotted against ζ and changes during the coalescence process should be read as ζ was decreasing from the largest to the smallest.

The number of H-bonds between all adsorbates and water molecules is plotted in Fig. 4a for sys. Tol-VP and Tol-VB and 4c for sys. Hep-VP and Hep-VB using symbols, and the dashed line with the same color represents the H-bonds between water and VO-79 only. The data reported here were for the adsorbates and the droplet they originally adhered to, before the SMD. That is, the H-bonding between adsorbates on one droplet and water in the other droplet was not considered here (to be discussed later), and hence the analysis allowed us to study how the coalescence disrupted the interaction and interfacial film within each droplet. As shown in Fig. 4a, the number of H-bonds between VO-79 and water was 96 in sys. Tol-VP, less than half of the value in sys. Tol-V (SI section SI6). The total number of H-bonds was over 1000 at the largest ζ; therefore, most H-bonds in sys. Tol-VP was between the SurP and water. The value gradually decreased as ζ became smaller, implying that the water-SurP interaction was compromised during coalescence. In sys. Tol-VB, even fewer H-bonds were formed between VO-79 and water, consistent with the distant peak of VO-79 found in Fig. 2b, while the total number of H-bonds was still greater than 1000 at the largest ζ. The presence of SurB weakened the interaction between VO-79 and water, but this was compensated by the large amount of H-bonds SurB established with water. The total H-bonds

also reduced slightly during the decrease of ζ. The reduction was less significant than that in sys. Tol-VP, indicating that the interaction between SurB and water was more stable. In heptane, the H-bonds between VO-79 and water were also supressed by the presence of the demulsifiers (Fig. 4c vs. data in SI section SI6 for the control sys. Hep-V). Compared with sys. Tol-VP, sys. Hep-VP in Fig. 4c had a similar amount of H-bonds between VO-79 and water, but the total number of H-bonds was higher, suggesting more H-bonds between SurP and water when heptane was the solvent. Consistently, the RDFs in Fig. 2c have shown a more compact interfacial film (narrower RDF peak) at the water/heptane interface than at the water/toluene interface (Fig. 2a). The number of H-bonds between VO-79 and water in sys. Hep-VB was similar to that in sys. Hep-VP, and higher than that in sys. Tol-VB. The total H-bonds between all adsorbates and water in sys. Hep-VB was the highest among the four systems, in line with Fig. 2d and SI section SI4 where the HP group of SurB was closest to water. During coalescence, the H-bonds between all adsorbates and water remained steady in Hep-VP and Hep-VB, and did not experience the decline observed for Tol-VP and Tol-VB. This is in line with Fig. 3 where during coalescence the surface redistribution of adsorbate molecules was less significant in heptane.

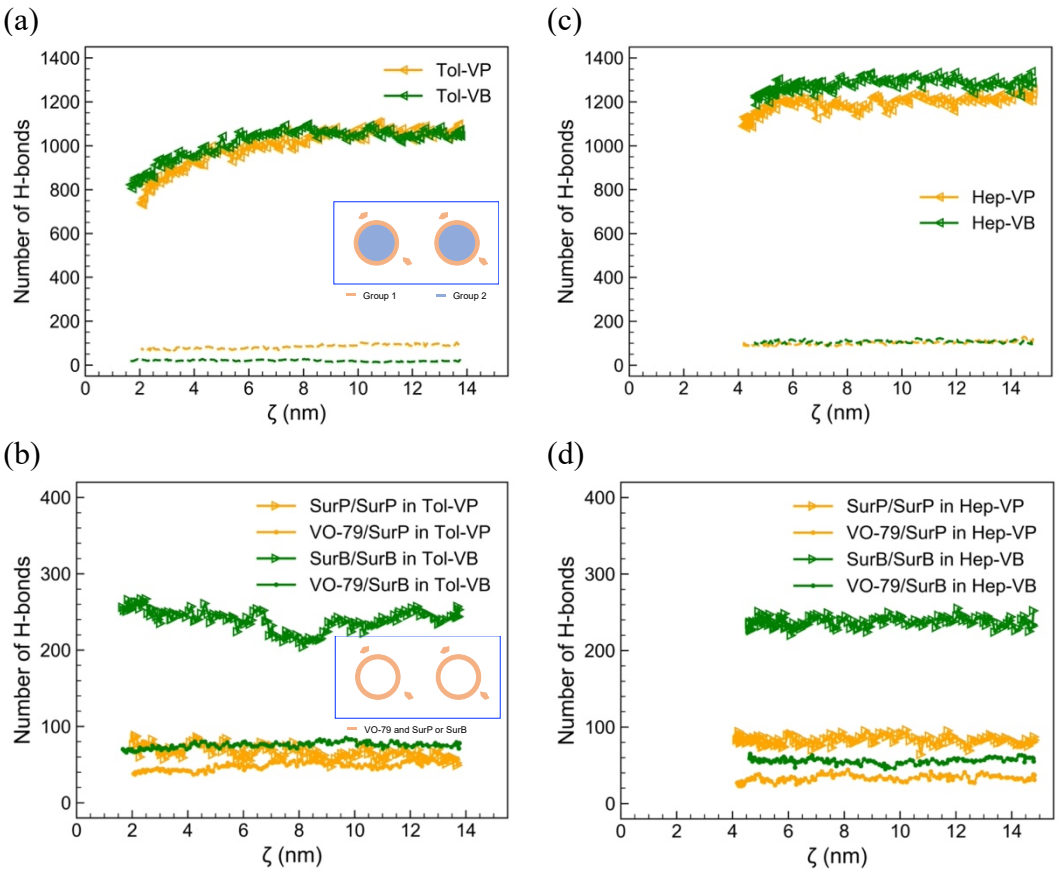

Figure 4. Number of H-bonds between adsorbates and water in (a) sys. Tol-VP and Tol-VB, (c) sys. Hep-VP and Hep-VB. Inset in subfigure (a) illustrates the two groups involved in H-bonding, group 1: adsorbates and group 2: water molecules. Solid curves with symbols are H-bonds between water and all adsorbate molecules (VO-79 and SurP or SurB), dashed curves are H-bonds between water and VO-79 only. Number of H-bonds within adsorbate films (i.e., among adsorbate molecules) in (b) sys. Tol-VP and Tol-VB, (d) sys. Hep-VP and Hep-VB. The groups involved in the H-bond calculation are illustrated in the inset of subfigure (b).

Fig. 4b and 4d shows the number of H-bonds between VO-79 and non-ionic surfactants (i.e., VO-79/SurP or VO-79/SurB) as well as between non-ionic surfactants themselves (i.e., SurP/SurP or SurB/SurB) within the adsorbate films. Similar to Fig. 4a and 4c, calculations here captured the

H-bonding among adsorbate molecules on the same droplets and from the two different droplets if they merged. As shown in Fig. 4b, there were similar H-bonds for SurP/SurP (55) and for VO-79/SurP (58) at the largest ζ in sys. Tol-VP. With the approaching of water droplets, the number of H-bonds for SurP/SurP gradually increased to 81 and that for VO-79/SurP decreased to 39. The coalescence disrupted the interaction between VO-79 and SurP and promoted the interaction between SurP themselves in the interfacial film. In Tol-VB, at the largest ζ the number of SurB/SurB H-bonds (248) was much higher than the number of VO-79/SurB H-bonds (76). As ζ decreased, the number of VO-79/SurB H-bonds remained steady; on the other hand, the number of SurB/SurB H-bonds decreased to the minimum of 204 at ζ~8.1 nm but increased to 256 at the lowest ζ,. Consulting Fig. 2b and Fig. 3b, the interaction between SurB themselves was dominant and remained relatively stable as the droplets approached each other. Overall, in toluene there were more H-bonds in the SurB/VO-79 film than in the SurP/VO-79 film. For sys. Hep-VP, as shown in Fig. 4d, the number of H-bonds for VO-79/SurP and SurP/SurP had no evident change with ζ, and the average values were 33 and 83 respectively. The total H-bonds within the VO-79/SurP film in sys. Hep-VP was similar to that in sys. Tol-VP, while the SurP/SurP H-bonds were more dominant in sys. Hep-VP. This is consistent with the observation that SurP formed a denser and thinner layer in heptane than in toluene (Fig. 2c vs. Fig. 2a and Fig. 3c vs. Fig. 3a). In sys. Hep-VB, the curve for VO-79/SurB H-bonds and SurB/SurB H-bonds were steady and remain at 56 and 237, respectively, which were slightly lower than that in sys. Tol-VB.

Upon the approaching of the two water droplets, the adsorbates were redistributed on the surface and in the regions where the two droplets faced each other. As a result, some water molecules became exposed to the organic solvent. In Fig. 5a-5d, the number of H-bonds between water molecules from two different droplets is plotted against ζ in cyan. In Fig. 5a-5b, for the range of ζ

from 14 nm to 6 nm, the number of H-bonds (cyan curves) was nearly zero for both sys. Tol-VP and Tol-VB. When ζ further reduced from 6 nm, the number of H-bonds became non-zero and started to increase drastically, indicating that the two water droplets started to merge. The onset of the increase occurred at higher ζ in sys. Tol-VB than in sys. Tol-VP, as shown in detail in the insets of Fig. 5a-5b. When ζ reached 2 nm (at the end of the SMD simulations), the two water droplets have merged into one and formed a large amount of H-bonds. For the systems in heptane (Fig. 5c-5d), the cyan curves also stayed at zero and then increased, while the onset of the increase occurred at lower ζ compared with sys. Tol-VP and Tol-VB.

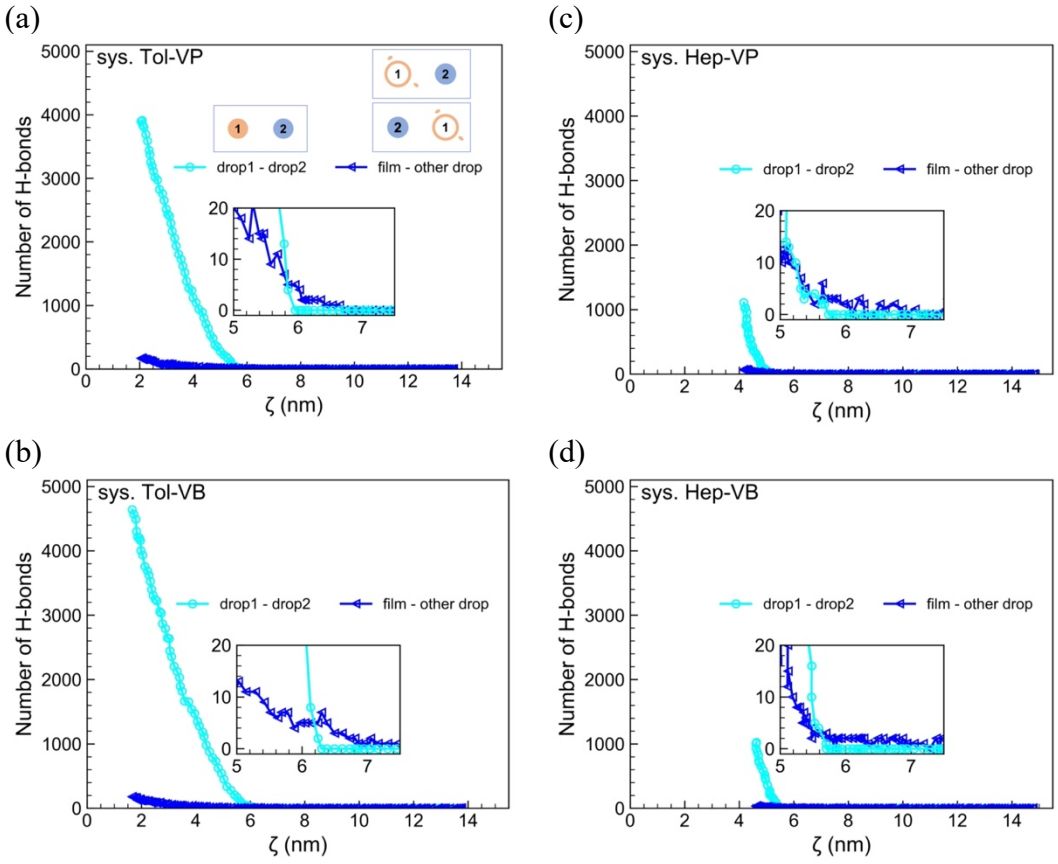

Figure 5. Number of H-bonds between water molecules from different droplets (drop1 – drop2) and between one water droplet and the adsorbate molecules in the other droplet (film – other drop) in (a) sys. Tol-VP, (b) Tol-VB, (c) sys. Hep-VP and (d) Hep-VB. The groups involved in the H-

bond calculation is illustrated in subfigure (a). The inset in each subfigure shows the details for ζ between 5 nm and 7.5 nm.

The snapshots in Fig. 3 suggested that the adsorbates on one droplet may interact with the other droplet and the adsorbates on it. Fig. 5a-5d (blue curves) shows the H-bonds between the adsorbates (group 1) and the water molecules of the other droplet (group 2). Both scenarios shown in the legend of Fig. 5a were considered and the data were the sum of the two. As shown in the inset of Fig. 5a for sys. Tol-VP, the blue curve had non-zero value for 6 nm < ζ < 7 nm, suggesting that the interfacial film had interacted with the exposed water surface before the two droplets were about to form H-bonds at ζ slightly lower than 6 nm (cyan curve). Similar feature was observed for sys. Tol-VB, Hep-VP and Hep-VB, where the interaction between adsorbates on one droplet and water in the other droplet started sooner, i.e., at larger ζ than the interaction between water molecules from the two droplets. Such a behavior was also observed in the control system Hep-V but absent in sys. Tol-V (SI section SI6). In the latter case, the VO-79 molecules formed negligible amount of H-bonds with water molecules in the other droplet until ζ reached around 4 nm, whereas the H-bond formation between two water droplets occurred at ζ = 6 nm. The result implies that in toluene and without the demulsifiers, VO-79 was able to easily redistribute on the droplet surface, exposing the water molecules, and drop coalescence was initiated by interactions among water molecules before the involvement of VO-79. While in this work, a complex interfacial film formed at the droplet surface, which reduced the ability of adsorbates to redistribute. On the other hand, the interfacial film played a role in bridging the two droplets in heptane, as well as in toluene with the presence of demulsifiers. In particular, in Fig. 5a-5b the blue curve for sys. Tol-VP was higher

than that for sys. Tol-VB when $\zeta < 6$ nm, indicating the higher tendency of SurP to bridge the droplets compared with SurB.

The aggregation of VO-79 (Fig. 6a and 6c) and demulsifiers (Fig. 6b and 6d) were analyzed by calculating the number of molecules in their largest aggregates. Here, a group of molecules were considered to form an aggregate if any molecule in this group had close contact with, i.e., within 0.35 nm of, at least one other molecule. With SurP or SurB adsorbed at the surface (Fig. 6a), sys. Tol-VP and Tol-VB had small VO-79 aggregates: the largest aggregate contained only about 20 molecules, as compared to ~107 molecules in the control sys. Tol-V (SI section SI7). The difference is significant even with the recognition that Tol-VP and Tol-VB contained less (104) VO-79 molecules than Tol-V (196). The values were stable with only subtle fluctuations, implying that the outer layer of the adsorbate film (VO-79) had no obvious association during the merging of the droplets. Instead, the association of SurP was significant in sys. Tol-VP, as shown in Fig. 6c. The number of molecules in the largest SurP aggregate was 95-97 at the largest ζ. Considering that the number of SurP molecules was 102 near each water droplet, most of them were interconnected on the surfaces of individual droplets. The value doubled at ζ~10 nm and dropped to 95 at ζ~7.5-9.2 nm. The increase was caused by the interaction and contact between adsorbate films on the two droplets, while the decrease was due to the instability of the interaction. The number doubled again when $\zeta < 7.5$ nm, corresponding to the merging of the two adsorbate films. The merging was not observed in sys. Tol-VB, where the number of molecules in the largest SurB aggregate only increased gradually with the decrease of ζ (Fig. 6b).

In sys. Hep-VP, the number of molecules in the largest VO-79 aggregate fluctuated between 21 and 32 (Fig. 6c), which may be attributed to unstable association of multiple small aggregates. This value was again much smaller than that (~272) in the control sys. Hep-V (SI section SI7).

The number of molecules in the largest SurP aggregate was 102 at large ζ (Fig. 6d), i.e., on each droplet all SurP molecules were interconnected and formed a single aggregate. The number doubled when ζ was slightly larger than 8 nm, suggesting the merging of the SurP aggregates. For sys. Hep-VB, the number of molecules in the largest VO-79 aggregate slightly increased during the reduction of ζ (Fig. 6c), while the curve for SurB fluctuated around 220, as shown in Fig. 6d.

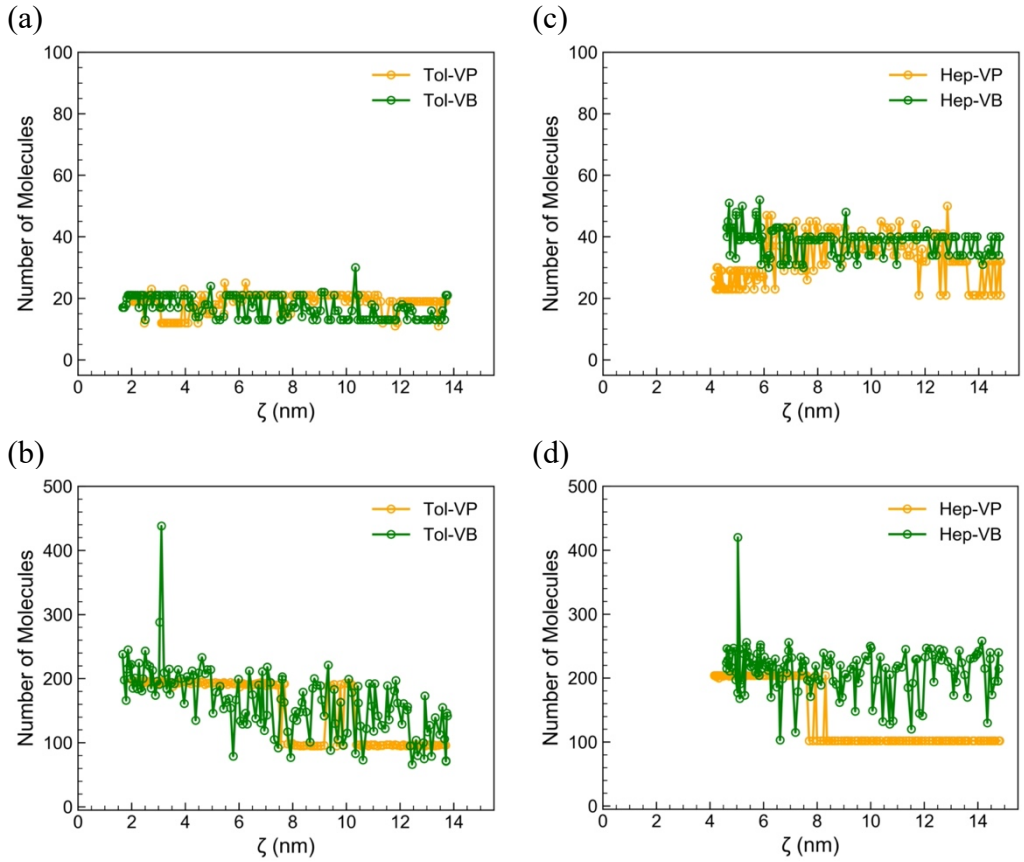

Figure 6. Number of molecules in the largest aggregate of VO-79 in (a) sys. Tol-VP and Tol-VB, and (c) sys. Hep-VP and Hep-VB. Number of molecules in the largest aggregate of the demulsifiers (SurP or SurB) in (b) sys. Tol-VP and Tol-VB, and (d) sys. Hep-VP and Hep-VB.

3.3 Free energy and mean force

PMF (ΔF) for water droplet coalescence was calculated through US simulations and plotted in Fig. 7a and 7c, where the PMF at the largest ζ (around 14 nm) was set to zero as the reference. As shown in Fig. 7a, the PMF value for sys. Tol-VP increased gradually as ζ decreased, representative of repulsive interaction between the droplets. The curve reached a maximum of ΔF_{max} = 93.8 kCal/mol at ζ = 6.82 nm. Over the energy barrier ΔF_{max}, PMF reduced as ζ further decreased suggesting attraction between the two droplets. Similar trend was observed for other systems, and the location and value of ΔF_{max} were marked on each curve in the form of (ζ (nm), ΔF_{max} (kCal/mol). The mean force between the droplets can be derived from the negative derivative of the PMF with respect to the reaction coordinate[59],

$$f(\zeta) = -\frac{\partial \Delta F}{\partial \zeta}. \quad (1)$$

Results for the mean force are shown in Fig. 7b and 7d, where positive value corresponds to repulsion and negative value corresponds to attraction. Each curve increased until a maximum (f_{max}) and then decreased upon further reduction in ζ. The location and value of f_{max} were also marked on each curve as (ζ (nm), f_{max} (pN)).

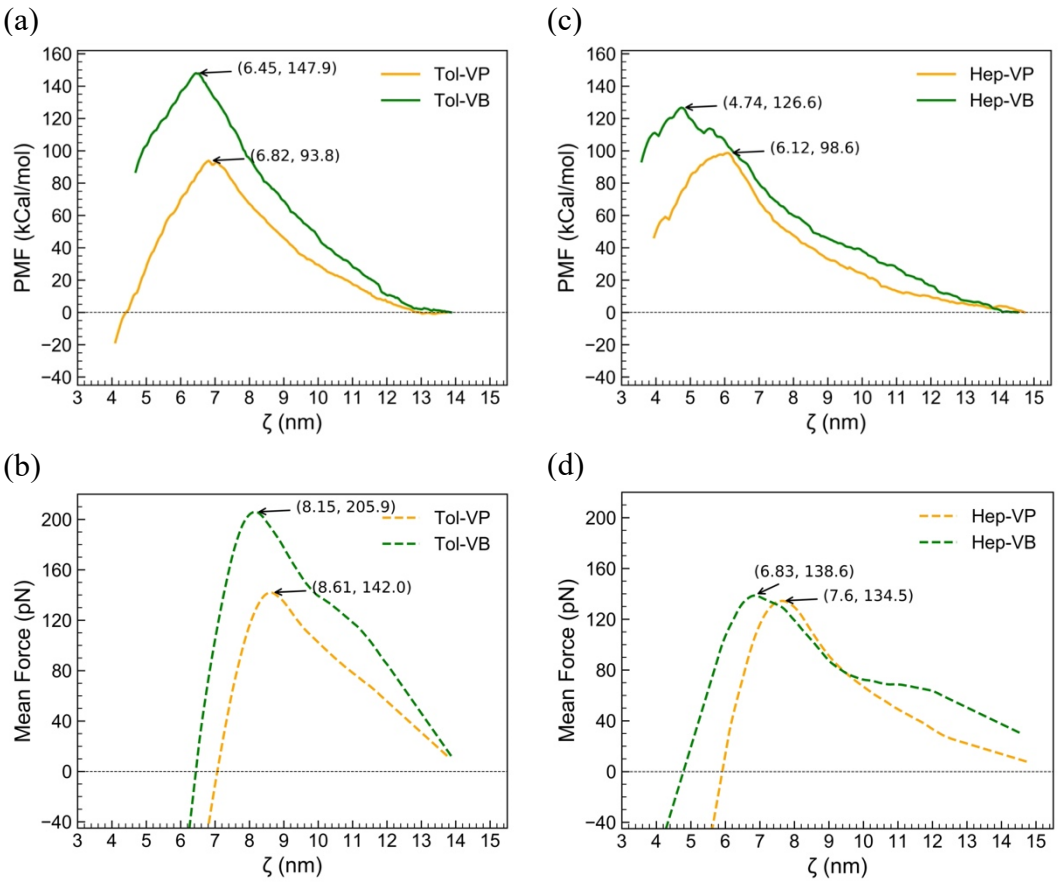

Figure 7. PMF during droplet coalescence for (a) sys. Tol-VP and Tol-VB, and (c) sys. Hep-VP and Hep-VB. Mean force during droplet coalescence for (b) sys. Tol-VP and Tol-VB, and (d) sys. Hep-VP and Hep-VB. Values in the parentheses are (ζ, PMF or mean force) at the maximum.

The coalescence process can be divided into three stages to facilitate the reading of the curves in Fig. 7a-d: stage 1 (ζ > 12.3 nm) where the interaction between the two droplets was low, stage 2 (from ζ = 12.3 nm to the PMF peak) where the droplets were under repulsion, and stage 3 (below the PMF peak) where the droplets attracted each other and coalesced. It should be noted that the value of ζ to divide stages 1 and 2 was only an estimate, where the change in PMF became more evident. In stage 1, the mean force in sys. Tol-VP (< 40 pN) was lower than that in the control sys. Tol-V (~50 pN)[31]. The reasons are two-fold. First, there were fewer VO-79 molecules in sys. Tol-

VP (104) compared with sys. Tol-V (196). Second, from the RDF (Fig. 2a) and snapshots (Fig. 3a), SurP had higher affinity to the water phase and replaced the VO-79 molecules at the droplet surface. With the co-adsorption of SurP and VO-79, the interfacial film had VO-79 located at the outer layer, which resulted in less dispersed VO-79 in sys. Tol-VP. Since dispersed VO-79 molecules pose a barrier for the approaching droplets[31], lower repulsion was found in Tol-VP than in sys. Tol-V. The observation was opposite in stage 2, where the curve for sys. Tol-VP increased to f_{max} ~ 140 pN, higher than that in sys. Tol-V (f_{max} ~ 98.2 pN)[31]. This can be attributed to the higher surface coverage provided by the co-adsorption of SurP and VO-79, which resulted in higher steric repulsion. In stage 3, the curve for Tol-VP was always higher than the curve for sys. Tol-V. Comparing sys. Tol-VB and Tol-VP, the force was higher in sys. Tol-VB in all stages. As suggested by the RDFs in Fig. 2b, a two-layer structure was formed by SurB and VO-79 was pushed to the outside of the second SurB layer. Such a thick structure led to steric hindrance at larger ζ and overall higher repulsion during the approaching of the water droplets.

Comparison of the systems in heptane showed similar characteristics, with the mean force following the general order of Hep-VB > Hep-VP > Hep-V (data in SI section SI8). The two-layer SurB structure again contributed to larger force and higher resistance to coalescence. Reading Fig. 7b and Fig. 7d together, the mean force was lower in heptane than in toluene. We attribute this to the fact that asphaltenes (represented by VO-79 here) are less soluble in heptane; they tend to form aggregates and adsorb at the water/heptane interface to minimize contact with heptane. Such features would facilitate the formation of attractive contact between the water droplets.

3.4 Discussion

Our previous work studied the coalescence of water droplets that were coated with a single component of adsorbates, either model asphaltene (VO-79) or non-ionic surfactants (SurP or SurB).[31] The results were shown to be in good agreement with AFM measurements.[31] Fundamentally, it verified the feasibility of this computational method for investigating W/O emulsion droplets. In this work, model asphaltenes and demulsifiers co-existed at the surface of the water droplets, which could provide more insights into the demulsification mechanisms. RDFs in Fig. 2 and snapshots in Fig. 3 confirmed that the demulsifier molecules were located closer to water than model asphaltenes, indicating that demulsifiers were able to replace asphaltenes at the interface. This replacement should be distinguished from "desorption" as asphaltenes may still be attached to the demulsifier film. Nevertheless, the structure of asphaltene film was indeed disrupted. For example, without non-ionic surfactants, VO-79 could form a large aggregate with 120 (out of the total of 196) interconnected molecules at the start of coalescence (SI section SI7). While with the addition of demulsifiers, the largest VO-79 aggregate contained only 20 to 40 (out of 104) molecules (Fig. 6a and 6c). The demulsification of W/O emulsions by non-ionic surfactants is commonly attributed to the higher affinity of the demulsifiers to the interface which enables them to replace the rigid asphaltene film.[22,35] While our results are consistent with this hypothesis, the additional atomistic details from our simulations allow us to visualize the structure of the adsorbate film containing asphaltene/demulsifier complexes, which is schematically shown in Fig. 8a-d.

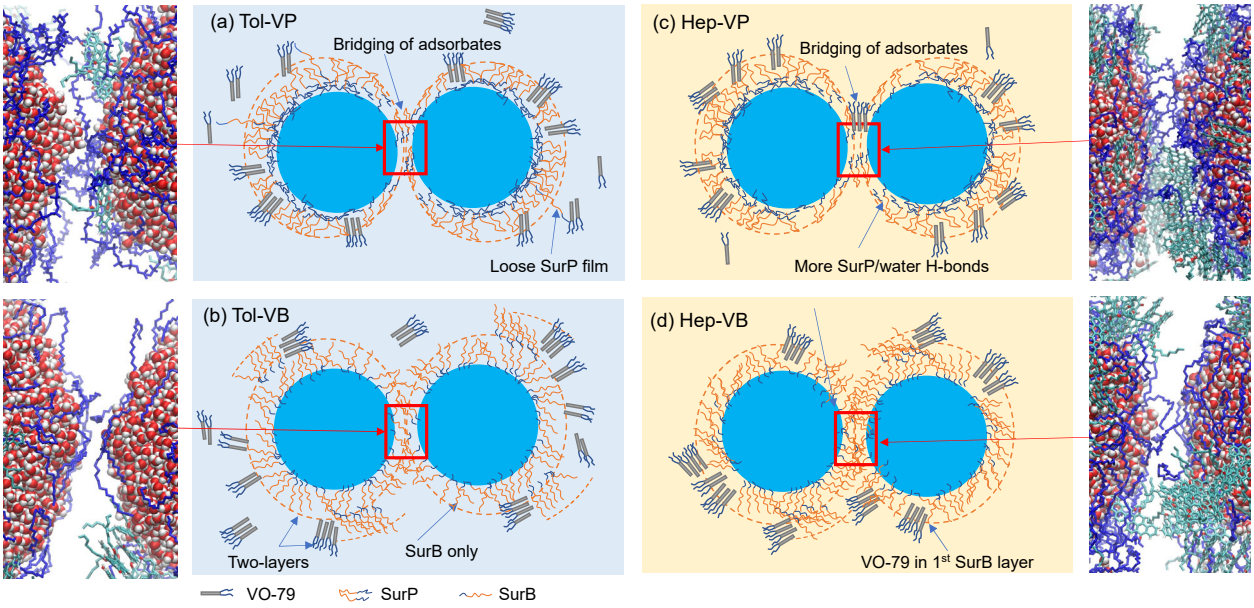

Figure 8. Schematics of the asphaltene/non-ionic surfactant interfacial film at the onset of droplet coalescence for sys. (a) Tol-VP, (b) Tol-VB, (c) Hep-VP, and (d) Hep-VB. Polyaromatic cores of VO-79 are shown as grey plates and their hydrophobic tails are in blue. For SurP and SurB, their hydrophilic groups are shown in blue and hydrophobic (lipophilic) groups in orange. Enlarged interfacial regions are accompanied by SMD simulation snapshots showing the bridging of adsorbate films at 0.8 ns in sys. Tol-VP and Tol-VB, and 0.9 ns for sys. Hep-VP and Hep-VB (red and white balls: oxygen and hydrogen in water; blue bonds: SurP or SurB; cyan bonds: VO-79).

In sys. Tol-VP (Fig. 8a), on each droplet surface, the SurP molecules adsorbed at the inner layer of the interfacial film and model asphaltenes were at the outer layer, with their hydrophilic groups oriented towards the water phase, as suggested by the RDF in Fig. 2a. Notably, due to their hydrophilic-hydrophobic-hydrophilic structure, the SurP molecules tended to bend and fold, exposing the hydrophobic center to toluene (Fig. 8a), with only a few exhibiting extended conformation into the oil phase (Fig. 3a). The radial location of VO-79 was similar to the

hydrophobic part of SurP (Fig. 2a). The adsorbate film was a complexation of VO-79 and SurP, confirmed by the formation of H-bonds between them (Fig. 4b). Within the film, SurP molecules also formed H-bonds between each other, and the amount was higher than that between VO-79 and SurP. The dominant interaction in the droplets, however, was the H-bonding between SurP molecules and water (Fig. 4a), which was higher than the H-bonds within the adsorbate film. During coalescence, the number of H-bonds between adsorbates and the droplet they originally adhered to decreased (Fig. 4a) while new H-bonds were formed with the other droplet (Fig. 5a). The adsorbate film established bridges (Fig. 5a) prior to the H-bond formation between water droplets, as illustrated in Fig. 8a. The SMD snapshot in Fig. 8a shows that the bridging was mainly attributed to SurP molecules that were not drained between the water droplets. Only VO-79 monomers and small aggregates were observed in the interfacial regions, and they were excluded from the thinnest part of the oil film.

In sys. Tol-VB (Fig. 8b), on each droplet surface SurB formed a two-layer structure (Fig. 2b). Their hydrophilic groups were also closer to the water phase, resulting in preferred orientation in the adsorbate film as illustrated in Fig. 8b. VO-79 molecules were almost completely excluded from the first layer of SurB, and there was no orientation preference for the hydrophobic and hydrophilic groups in VO-79 (Fig. 2b). Though with only two EO units and one hydroxyl unit, the hydrophilic tail of SurB formed considerable amount of H-bonds with water which did not decrease as much as in sys. Tol-VP during droplet coalescence (Fig. 4a). This indicates that the adsorbate film was more stably bonded to water in sys. Tol-VB than in sys. Tol-VP. The thicker two-layer structure and more stable adsorbate film contributed to the larger repulsive force during droplet coalescence in Tol-VB (Fig. 7b). The snapshot in Fig. 8b also suggested that bridging was primarily enabled by SurB molecules, as VO-79 were drained from the thinnest part of the oil film.

Asphaltenes are defined as the fraction of crude oil that is soluble in aromatic solvents (e.g., toluene) and insoluble in n-alkanes (e.g., heptane).[60] The property of the solvent that represents the oil phase is an important factor that affects the stability of W/O emulsion droplets. As stated by Qiao et al.[61], the majority of the water droplets stabilized by interfacial-active asphaltenes (IAA) were smaller in toluene than in heptol (heptane/toluene 1:1 vol.), suggesting a higher resistance to coalescence in toluene. The AFM measurements of Shi et al. also suggested that in pure heptane, the adhesion between asphaltene film promoted the coalescence of water droplets.[4] In our work, the energy barrier (29.4 kCal/mol) and maximum force (33.0 pN) in sys. Hep-V was lower than 70.3 kCal/mol and 98.2 pN in sys. Tol-V[31], which is consistent with Qiao et al.[61] and Shi et al.[4] The characteristics of the VO-79/SurP film were preserved when the solvent was changed from toluene to heptane, as shown in Fig. 8a and 8c. While with lower solubility of VO-79 in heptane, two differences are worth highlighting. On the one hand, the extended conformation of some surface SurP molecules in sys. Tol-VP (Fig. 3a) was absent in sys. Hep-VP (Fig. 3c), and more SurP/water H-bonds were formed in Hep-VP (Fig. 4c vs. 4a). Such a feature resulted in a more tightly bound SurP layer, which tended to reduce the exposure of water molecules for coalescence and increase the repulsion in Hep-VP. On the other hand, VO-79 formed larger aggregates in sys. Hep-VP (Fig. 6c) than in Tol-VP (Fig. 6a). Such large VO-79 aggregates stayed in the oil film between water droplets and participated in bridging (Fig. 8c), which tended to reduce the repulsion for coalescence. The competition between the two effects is likely the reason why the difference in energy barrier or mean force was insignificant for sys. Tol-VP and Hep-VP (Fig. 7a, c). The formation of a two-layer structure by SurB was present in both Tol-VB and Hep-VB (Fig. 8b and 8d). Similar to SurP, in heptane more SurB molecules were adsorbed in the first layer (higher first RDF peak in Fig. 2d than in Fig. 2b) and formed more SurB/water H-bonds (Fig. 4c vs. 4a), which

tended to increase the repulsion for coalescence. However, in heptane VO-79 molecules also moved towards the first layer (Fig. 2d vs. 2b), which could reduce the steric repulsion from the bulky VO-79 in the outer layer as seen in Fig. 3b. In addition, similar to sys. Hep-VP, VO-79 aggregates in sys. Hep-VB stayed in the oil film between the water droplets and participated in their bridging (snapshot in Fig. 8d). The net consequence was a significant reduction of repulsion in heptane (Fig. 7d vs. 7b).

In real crude oil, asphaltenes are a complex mixture, and it is commonly believed that water-in-crude oil droplets are covered by a rigid film formed by various surface-active components.[62,63] Zhang et al. reported that compared with VO-79, crude oil derived asphaltenes resulted in finer sized water droplets in oil (toluene) and more stable W/O emulsions.[34] In the control systems where VO-79 was the only adsorbate, the water/oil interface was partially covered by a patchy VO-79 film (SI section SI5), even when the mass concentration of VO-79 was as high as 10 wt.% (Table 1). For a given type of solvent, the control system had the lowest energy barrier and repulsive force (previous work[31] and SI section SI8), followed by the system with a loose VO-79/SurP film and then the system with a condensed VO-79/SurB film. Our results therefore revealed that the interaction force for droplet coalescence was highly dependent on the structure of the interfacial film. Crude oil derived asphaltenes contain a mixture of molecules with various architectures, polarity, and interfacial affinity, which likely will form a more rigid and compact film at the interface compared with VO-79. As a result, the water droplets in crude oil could have much higher repulsion and stability than the system with a single model asphaltene. One could expect that SurP might produce a looser structure than the rigid asphaltene film in crude oil and reduce the repulsion during droplet coalescence.

Finally, we mention limitations of this work and several important aspects that can be studied in the future. Firstly, while the model asphaltene VO-79 captures some structural characteristics of continental asphaltenes, real asphaltene molecules can have different polyaromatic cores, molecular weight, heteroatoms and polarity. These differences can affect the stability of W/O emulsion droplets in future investigations where a more comprehensive representation of real asphaltene is sought. Secondly, stability of the emulsion droplets can be size-dependent. While the systems simulated in this work are quite large compared with other all-atom MD simulations in the literatures[1,30], the droplets are still in the nanometer range. Coarse-graining and/or other simulation techniques should be considered for micrometer-sized droplets, but care needs to be taken in order not to lose the important molecular details for the interfacial interactions. Thirdly, the PMF calculated in this work describes the change in free energy during droplet coalescence, which includes both energetic and entropic contributions. The change of H-bonds during droplet coalescence, computed in this work between different components, is a manifestation of the intermolecular interactions and associated free energy change. Accurate decomposition of the free energy into energetic and entropic components is non-trivial due to the fluctuation in the total energy of the system along the simulation trajectory. Other techniques may be employed, e.g., by studying the dependence of the free energy change on temperature, but this would involve a significant amount of additional simulations. Nevertheless, such a decomposition would provide valuable insights into the driving force for water droplet coalescence.

4. Conclusions

In this work, MD simulations were performed to probe the coalescence of W/O emulsion droplets with the presence of both model asphaltene and demulsifiers. Free energy and interaction

force between such droplets during coalescence were calculated for the *first* time via PMF calculations. Based on the simulation data, we proposed the structures of the interfacial film, which varied with the type of demulsifier and solvent, and played an important role in the interaction force during droplet coalescence. Both demulsifiers adsorbed closer to the water phase compared to the model asphaltene and disrupted the formation of large asphaltene aggregates. While the triblock polymer and VO-79 formed a single-layer film on the droplet surface, a two-layer structure was formed in the presence of Brij surfactant, regardless of the type of solvent. This thick two-layer structure contributed to higher repulsion during droplet coalescence. Given a specific demulsifier, the interfacial film was thinner in heptane than in toluene, due to the poorer solubility of VO-79 in heptane and the resulting tendency to form a more compact structure on the droplet surface. Consequently, lower repulsive force was found in heptane when compared with the counterpart in toluene (except for the case with the triblock polymer where the repulsive force was comparable in the two solvents). This work revealed that the interaction force during droplet coalescence was highly dependent on the structure of interfacial film on the droplet surface, which provided atomic-level insights into the demulsification mechanisms.

Supporting Information

Partial atomic charge of surfactants (SI1); Time evolution of COM separation during SMD (SI2); Details of umbrella sampling (SI3); Additional RDF and details of RDF peaks (SI4); Configurations of SMD for sys. Tol-V and sys. Hep-V (SI5); Number of H-bonds in control systems (SI6); Aggregate size of VO-79 in control systems (SI7); PMF and mean force for control system Hep-V (SI8).

Declaration of Competing Interest

The authors declare that they have no known competing financial interests or personal relationships that could have appeared to influence the work reported in this paper.

Acknowledgements

The authors gratefully acknowledge the computing resources and technical support from Digital Research Alliance of Canada, and the financial support from the Natural Sciences and Engineering Research Council of Canada (NSERC), Canada Research Chairs Program, Syncrude Canada Ltd., Suncor Energy, Canadian Natural Resources Limited, ChampionX, and the Future Energy Systems under the Canada First Research Excellence Fund.

References

(1) Pak, C. Y.; Li, W.; Steve Tse, Y.-L. Free Energy and Dynamics of Water Droplet Coalescence. *J. Phys. Chem. C* **2018**, *122* (40), 22975–22984. https://doi.org/10.1021/acs.jpcc.8b06507.

(2) Focke, C.; Kuschel, M.; Sommerfeld, M.; Bothe, D. Collision between High and Low Viscosity Droplets: Direct Numerical Simulations and Experiments. *International Journal of Multiphase Flow* **2013**, *56*, 81–92. https://doi.org/10.1016/j.ijmultiphaseflow.2013.05.008.

(3) Zhang, Y. R.; Jiang, X. Z.; Luo, K. H. Bounce Regime of Droplet Collisions: A Molecular Dynamics Study. *Journal of Computational Science* **2016**, *17*, 457–462. https://doi.org/10.1016/j.jocs.2016.03.011.

(4) Shi, C.; Zhang, L.; Xie, L.; Lu, X.; Liu, Q.; He, J.; Mantilla, C. A.; Van den berg, F. G. A.; Zeng, H. Surface Interaction of Water-in-Oil Emulsion Droplets with Interfacially Active Asphaltenes. *Langmuir* **2017**, *33* (5), 1265–1274. https://doi.org/10.1021/acs.langmuir.6b04265.

(5) Gafonova, O. V.; Yarranton, H. W. The Stabilization of Water-in-Hydrocarbon Emulsions by Asphaltenes and Resins. *Journal of Colloid and Interface Science* **2001**, *241* (2), 469–478. https://doi.org/10.1006/jcis.2001.7731.

(6) Mettu, S.; Wu, C.; Dagastine, R. R. Dynamic Forces between Emulsified Water Drops Coated with Poly-Glycerol-Poly-Ricinoleate (PGPR) in Canola Oil. *Journal of Colloid and Interface Science* **2018**, *517*, 166–175. https://doi.org/10.1016/j.jcis.2018.01.104.

(7) Kilpatrick, P. K. Water-in-Crude Oil Emulsion Stabilization: Review and Unanswered Questions. *Energy Fuels* **2012**, *26* (7), 4017–4026. https://doi.org/10.1021/ef3003262.

(8) Andrews, A. B.; McClelland, A.; Korkeila, O.; Demidov, A.; Krummel, A.; Mullins, O. C.; Chen, Z. Molecular Orientation of Asphaltenes and PAH Model Compounds in Langmuir−Blodgett Films Using Sum Frequency Generation Spectroscopy. *Langmuir* **2011**, *27* (10), 6049–6058. https://doi.org/10.1021/la200466b.

(9) Xie, L.; Lu, Q.; Tan, X.; Liu, Q.; Tang, T.; Zeng, H. Interfacial Behavior and Interaction Mechanism of Pentol/Water Interface Stabilized with Asphaltenes. *Journal of Colloid and Interface Science* **2019**, *553*, 341–349. https://doi.org/10.1016/j.jcis.2019.06.035.

(10) McLean, J. D.; Kilpatrick, P. K. Effects of Asphaltene Solvency on Stability of Water-in-Crude-Oil Emulsions. *Journal of Colloid and Interface Science* **1997**, *189* (2), 242–253. https://doi.org/10.1006/jcis.1997.4807.

(11) Li, T.; Li, M.; Zhang, L.; Yan, M.; Li, H. Molecular Dynamics Study of the Temperature-Dependent Coalescence of Liquid Nanodrops: Implications for Microfluidics. *ACS Appl. Nano Mater.* **2019**, *2* (12), 7978–7988. https://doi.org/10.1021/acsanm.9b02018.

(12) Cheng, L.-C.; Hashemnejad, S. M.; Zarket, B.; Muthukrishnan, S.; Doyle, P. S. Thermally and PH-Responsive Gelation of Nanoemulsions Stabilized by Weak Acid Surfactants. *Journal of Colloid and Interface Science* **2020**, *563*, 229–240. https://doi.org/10.1016/j.jcis.2019.12.054.

(13) Liao, M.-L.; Ju, S.-P.; Yang, S.-H. Coalescence Behavior of Water Nanoclusters: Temperature and Size Effects. *J. Phys. Chem. C* **2007**, *111* (19), 6927–6932. https://doi.org/10.1021/jp066246t.

(14) Borges, B.; Rondón, M.; Sereno, O.; Asuaje, J. Breaking of Water-in-Crude-Oil Emulsions. 3. Influence of Salinity and Water−Oil Ratio on Demulsifier Action. *Energy Fuels* **2009**, *23* (3), 1568–1574. https://doi.org/10.1021/ef8008822.

(15) Fortuny, M.; Oliveira, C. B. Z.; Melo, R. L. F. V.; Nele, M.; Coutinho, R. C. C.; Santos, A. F. Effect of Salinity, Temperature, Water Content, and PH on the Microwave Demulsification of Crude Oil Emulsions †. *Energy Fuels* **2007**, *21* (3), 1358–1364. https://doi.org/10.1021/ef0603885.
(16) Jian, C.; Poopari, M. R.; Liu, Q.; Zerpa, N.; Zeng, H.; Tang, T. Mechanistic Understanding of the Effect of Temperature and Salinity on the Water/Toluene Interfacial Tension. *Energy Fuels* **2016**, *30* (12), 10228–10235. https://doi.org/10.1021/acs.energyfuels.6b01995.
(17) Abullah, M. M. S.; Al-Lohedan, H. A.; Attah, A. M. Synthesis and Application of Amphiphilic Ionic Liquid Based on Acrylate Copolymers as Demulsifier and Oil Spill Dispersant. *Journal of Molecular Liquids* **2016**, *219*, 54–62. https://doi.org/10.1016/j.molliq.2016.03.011.
(18) Daniel-David, D.; Le Follotec, A.; Pezron, I.; Dalmazzone, C.; Noïk, C.; Barré, L.; Komunjer, L. Destabilisation of Water-in-Crude Oil Emulsions by Silicone Copolymer Demulsifiers. *Oil & Gas Science and Technology - Rev. IFP* **2008**, *63* (1), 165–173. https://doi.org/10.2516/ogst:2008002.
(19) Abdulredha, M. M.; Hussain, S. A.; Abdullah, L. C. Separation Emulsion via Non-Ionic Surfactant: An Optimization. *Processes* **2019**, *7* (6), 382. https://doi.org/10.3390/pr7060382.
(20) Adilbekova, A. O.; Omarova, K. I.; Karakulova, A.; Musabekov, K. B. Nonionic Surfactants Based on Polyoxyalkylated Copolymers Used as Demulsifying Agents. *Colloids and Surfaces A: Physicochemical and Engineering Aspects* **2015**, *480*, 433–438. https://doi.org/10.1016/j.colsurfa.2014.11.004.
(21) Pensini, E.; Harbottle, D.; Yang, F.; Tchoukov, P.; Li, Z.; Kailey, I.; Behles, J.; Masliyah, J.; Xu, Z. Demulsification Mechanism of Asphaltene-Stabilized Water-in-Oil Emulsions by a Polymeric Ethylene Oxide–Propylene Oxide Demulsifier. *Energy Fuels* **2014**, *28* (11), 6760–6771. https://doi.org/10.1021/ef501387k.
(22) Shehzad, F.; Hussein, I. A.; Kamal, M. S.; Ahmad, W.; Sultan, A. S.; Nasser, M. S. Polymeric Surfactants and Emerging Alternatives Used in the Demulsification of Produced Water: A Review. *Polymer Reviews* **2018**, *58* (1), 63–101. https://doi.org/10.1080/15583724.2017.1340308.
(23) Wang, D.; Zhao, Z.; Qiao, C.; Yang, W.; Huang, Y.; McKay, P.; Yang, D.; Liu, Q.; Zeng, H. Techniques for Treating Slop Oil in Oil and Gas Industry: A Short Review. *Fuel* **2020**, *279*, 118482. https://doi.org/10.1016/j.fuel.2020.118482.
(24) Kamp, J.; Villwock, J.; Kraume, M. Drop Coalescence in Technical Liquid/Liquid Applications: A Review on Experimental Techniques and Modeling Approaches. *Reviews in Chemical Engineering* **2017**, *33* (1), 1–47. https://doi.org/10.1515/revce-2015-0071.
(25) Mohammadi, M.; Shahhosseini, S.; Bayat, M. Direct Numerical Simulation of Water Droplet Coalescence in the Oil. *International Journal of Heat and Fluid Flow* **2012**, *36*, 58–71. https://doi.org/10.1016/j.ijheatfluidflow.2012.04.001.
(26) Chen, Y.; Shen, C.; Peterson, G. P. Hydrodynamics and Morphologies of Droplet Coalescence. *Ind. Eng. Chem. Res.* **2015**, *54* (37), 9257–9262. https://doi.org/10.1021/acs.iecr.5b01459.
(27) Perumanath, S.; Borg, M. K.; Chubynsky, M. V.; Sprittles, J. E.; Reese, J. M. Droplet Coalescence Is Initiated by Thermal Motion. *Phys. Rev. Lett.* **2019**, *122* (10), 104501. https://doi.org/10.1103/PhysRevLett.122.104501.

(28) Dagastine, R. R.; Stevens, G. W.; Chan, D. Y. C.; Grieser, F. Forces between Two Oil Drops in Aqueous Solution Measured by AFM. *Journal of Colloid and Interface Science* **2004**, *273* (1), 339–342. https://doi.org/10.1016/j.jcis.2003.11.001.
(29) Carnie, S. L.; Chan, D. Y. C.; Lewis, C.; Manica, R.; Dagastine, R. R. Measurement of Dynamical Forces between Deformable Drops Using the Atomic Force Microscope. I. Theory. *Langmuir* **2005**, *21* (7), 2912–2922. https://doi.org/10.1021/la0475371.
(30) Pak, C. Y.; Li, W.; Steve Tse, Y.-L. Free Energy and Dynamics of Organic-Coated Water Droplet Coalescence. *J. Phys. Chem. C* **2020**, *124* (16), 8749–8757. https://doi.org/10.1021/acs.jpcc.0c00175.
(31) Sun, X.; Yang, D.; Zhang, H.; Zeng, H.; Tang, T. Unraveling the Interaction of Water-in-Oil Emulsion Droplets via Molecular Simulations and Surface Force Measurements. *J. Phys. Chem. B* **2021**, *125* (27), 7556–7567. https://doi.org/10.1021/acs.jpcb.1c04227.
(32) López-Linares, F.; Carbognani, L.; González, M. F.; Sosa-Stull, C.; Figueras, M.; Pereira-Almao, P. Quinolin-65 and Violanthrone-79 as Model Molecules for the Kinetics of the Adsorption of C7 Athabasca Asphaltene on Macroporous Solid Surfaces. *Energy Fuels* **2006**, *20* (6), 2748–2750. https://doi.org/10.1021/ef060354x.
(33) Mullins, O. C.; Sabbah, H.; Eyssautier, J.; Pomerantz, A. E.; Barré, L.; Andrews, A. B.; Ruiz-Morales, Y.; Mostowfi, F.; McFarlane, R.; Goual, L.; Lepkowicz, R.; Cooper, T.; Orbulescu, J.; Leblanc, R. M.; Edwards, J.; Zare, R. N. Advances in Asphaltene Science and the Yen–Mullins Model. *Energy Fuels* **2012**, *26* (7), 3986–4003. https://doi.org/10.1021/ef300185p.
(34) Zhang, Z.; Song, J.; Lin, Y.-J.; Wang, X.; Biswal, S. L. Comparing the Coalescence Rate of Water-in-Oil Emulsions Stabilized with Asphaltenes and Asphaltene-like Molecules. *Langmuir* **2020**, *36* (27), 7894–7900. https://doi.org/10.1021/acs.langmuir.0c00966.
(35) Wang, D.; Yang, D.; Huang, C.; Huang, Y.; Yang, D.; Zhang, H.; Liu, Q.; Tang, T.; Gamal El-Din, M.; Kemppi, T.; Perdicakis, B.; Zeng, H. Stabilization Mechanism and Chemical Demulsification of Water-in-Oil and Oil-in-Water Emulsions in Petroleum Industry: A Review. *Fuel* **2021**, *286*, 119390. https://doi.org/10.1016/j.fuel.2020.119390.
(36) Kailey, I.; Feng, X. Influence of Structural Variations of Demulsifiers on Their Performance. *Ind. Eng. Chem. Res.* **2013**, *52* (2), 785–793. https://doi.org/10.1021/ie3028137.
(37) Guo, X.; Rong, Z.; Ying, X. Calculation of Hydrophile–Lipophile Balance for Polyethoxylated Surfactants by Group Contribution Method. *Journal of Colloid and Interface Science* **2006**, *298* (1), 441–450. https://doi.org/10.1016/j.jcis.2005.12.009.
(38) Pradilla, D.; Simon, S.; Sjöblom, J. Mixed Interfaces of Asphaltenes and Model Demulsifiers, Part II: Study of Desorption Mechanisms at Liquid/Liquid Interfaces. *Energy Fuels* **2015**, *29* (9), 5507–5518. https://doi.org/10.1021/acs.energyfuels.5b01302.
(39) Pradilla, D.; Simon, S.; Sjöblom, J. Mixed Interfaces of Asphaltenes and Model Demulsifiers Part I: Adsorption and Desorption of Single Components. *Colloids and Surfaces A: Physicochemical and Engineering Aspects* **2015**, *466*, 45–56. https://doi.org/10.1016/j.colsurfa.2014.10.051.
(40) Sun, X.; Zeng, H.; Tang, T. Effect of Non-Ionic Surfactants on the Adsorption of Polycyclic Aromatic Compounds at Water/Oil Interface: A Molecular Simulation Study. *Journal of Colloid and Interface Science* **2021**, *586*, 766–777. https://doi.org/10.1016/j.jcis.2020.10.146.

(41) Lan, T.; Zeng, H.; Tang, T. Understanding Adsorption of Violanthrone-79 as a Model Asphaltene Compound on Quartz Surface Using Molecular Dynamics Simulations. *J. Phys. Chem. C* **2018**, *122* (50), 28787–28796. https://doi.org/10.1021/acs.jpcc.8b09712.
(42) Lan, T.; Zeng, H.; Tang, T. Molecular Dynamics Study on the Mechanism of Graphene Oxide to Destabilize Oil/Water Emulsion. *J. Phys. Chem. C* **2019**, *123* (37), 22989–22999. https://doi.org/10.1021/acs.jpcc.9b05906.
(43) Frisch, M. J.; Trucks, G. W.; Schlegel, H. B.; Scuseria, G. E.; Robb, M. A.; Cheeseman, J. R.; Scalmani, G.; Barone, V.; Petersson, G. A.; Nakatsuji, H.; Li, X.; Caricato, M.; Marenich, A. V.; Bloino, J.; Janesko, B. G.; Gomperts, R.; Mennucci, B.; Hratchian, H. P.; Ortiz, J. V.; Izmaylov, A. F.; Sonnenberg, J. L.; Williams; Ding, F.; Lipparini, F.; Egidi, F.; Goings, J.; Peng, B.; Petrone, A.; Henderson, T.; Ranasinghe, D.; Zakrzewski, V. G.; Gao, J.; Rega, N.; Zheng, G.; Liang, W.; Hada, M.; Ehara, M.; Toyota, K.; Fukuda, R.; Hasegawa, J.; Ishida, M.; Nakajima, T.; Honda, Y.; Kitao, O.; Nakai, H.; Vreven, T.; Throssell, K.; Montgomery Jr., J. A.; Peralta, J. E.; Ogliaro, F.; Bearpark, M. J.; Heyd, J. J.; Brothers, E. N.; Kudin, K. N.; Staroverov, V. N.; Keith, T. A.; Kobayashi, R.; Normand, J.; Raghavachari, K.; Rendell, A. P.; Burant, J. C.; Iyengar, S. S.; Tomasi, J.; Cossi, M.; Millam, J. M.; Klene, M.; Adamo, C.; Cammi, R.; Ochterski, J. W.; Martin, R. L.; Morokuma, K.; Farkas, O.; Foresman, J. B.; Fox, D. J. Gaussian 16 Rev. C.01, 2016.
(44) Becke, A. D. A New Mixing of Hartree–Fock and Local Density-functional Theories. *The Journal of Chemical Physics* **1993**, *98* (2), 1372–1377. https://doi.org/10.1063/1.464304.
(45) Malde, A. K.; Zuo, L.; Breeze, M.; Stroet, M.; Poger, D.; Nair, P. C.; Oostenbrink, C.; Mark, A. E. An Automated Force Field Topology Builder (ATB) and Repository: Version 1.0. *J. Chem. Theory Comput.* **2011**, *7* (12), 4026–4037. https://doi.org/10.1021/ct200196m.
(46) Breneman, C. M.; Wiberg, K. B. Determining Atom-Centered Monopoles from Molecular Electrostatic Potentials. The Need for High Sampling Density in Formamide Conformational Analysis. *Journal of Computational Chemistry* **1990**, *11* (3), 361–373. https://doi.org/10.1002/jcc.540110311.
(47) Berendsen, H. J.; Postma, J. P.; van Gunsteren, W. F.; Hermans, J. Interaction Models for Water in Relation to Protein Hydration. In *Intermolecular forces*; Springer, 1981; pp 331–342.
(48) Jian, C.; Tang, T. Molecular Dynamics Simulations Reveal Inhomogeneity-Enhanced Stacking of Violanthrone-78-Based Polyaromatic Compounds in *n* -Heptane–Toluene Mixtures. *J. Phys. Chem. B* **2015**, *119* (27), 8660–8668. https://doi.org/10.1021/acs.jpcb.5b04481.
(49) Spoel, D. V. D.; Lindahl, E.; Hess, B.; Groenhof, G.; Mark, A. E.; Berendsen, H. J. C. GROMACS: Fast, Flexible, and Free. *Journal of Computational Chemistry* **2005**, *26* (16), 1701–1718. https://doi.org/10.1002/jcc.20291.
(50) Lindahl, E.; Hess, B.; van der Spoel, D. Gromacs 3.0: A Package for Molecular Simulation and Trajectory Analysis. *J Mol Model* **2001**, *7* (8), 306–317. https://doi.org/10.1007/s008940100045.
(51) Berendsen, H. J. C.; van der Spoel, D.; van Drunen, R. Gromacs: A Message-Passing Parallel Molecular Dynamics Implementation. *Computer Physics Communications* **1995**, *91* (1–3), 43–56. https://doi.org/10.1016/0010-4655(95)00042-E.

(52) Oostenbrink, C.; Villa, A.; Mark, A. E.; Gunsteren, W. F. V. A Biomolecular Force Field Based on the Free Enthalpy of Hydration and Solvation: The Gromos Force-Field Parameter Sets 53a5 and 53a6. *Journal of Computational Chemistry* **2004**, *25* (13), 1656–1676. https://doi.org/10.1002/jcc.20090.
(53) Saito, H.; Nagao, H.; Nishikawa, K.; Kinugawa, K. Molecular Collective Dynamics in Solid Para-Hydrogen and Ortho-Deuterium: The Parrinello–Rahman-Type Path Integral Centroid Molecular Dynamics Approach. *The Journal of Chemical Physics* **2003**, *119* (2), 953–963. https://doi.org/10.1063/1.1578474.
(54) Hess, B. P-LINCS: A Parallel Linear Constraint Solver for Molecular Simulation. *J. Chem. Theory Comput.* **2008**, *4* (1), 116–122. https://doi.org/10.1021/ct700200b.
(55) Essmann, U.; Perera, L.; Berkowitz, M. L.; Darden, T.; Lee, H.; Pedersen, L. G. A Smooth Particle Mesh Ewald Method. *The Journal of Chemical Physics* **1995**, *103* (19), 8577–8593. https://doi.org/10.1063/1.470117.
(56) Sevick, E. M.; Monson, P. A.; Ottino, J. M. Monte Carlo Calculations of Cluster Statistics in Continuum Models of Composite Morphology. *The Journal of Chemical Physics* **1988**, *88* (2), 1198–1206. https://doi.org/10.1063/1.454720.
(57) Lemkul, J. A.; Bevan, D. R. Assessing the Stability of Alzheimer's Amyloid Protofibrils Using Molecular Dynamics. *J. Phys. Chem. B* **2010**, *114* (4), 1652–1660. https://doi.org/10.1021/jp9110794.
(58) Hub, J. S.; de Groot, B. L.; van der Spoel, D. G_wham—A Free Weighted Histogram Analysis Implementation Including Robust Error and Autocorrelation Estimates. *J. Chem. Theory Comput.* **2010**, *6* (12), 3713–3720. https://doi.org/10.1021/ct100494z.
(59) Kopelevich, D. I. One-Dimensional Potential of Mean Force Underestimates Activation Barrier for Transport across Flexible Lipid Membranes. *The Journal of Chemical Physics* **2013**, *139* (13), 134906. https://doi.org/10.1063/1.4823500.
(60) Headen, T. F.; Boek, E. S.; Jackson, G.; Totton, T. S.; Müller, E. A. Simulation of Asphaltene Aggregation through Molecular Dynamics: Insights and Limitations. *Energy Fuels* **2017**, *31* (2), 1108–1125. https://doi.org/10.1021/acs.energyfuels.6b02161.
(61) Qiao, P.; Harbottle, D.; Tchoukov, P.; Wang, X.; Xu, Z. Asphaltene Subfractions Responsible for Stabilizing Water-in-Crude Oil Emulsions. Part 3. Effect of Solvent Aromaticity. *Energy Fuels* **2017**, *31* (9), 9179–9187. https://doi.org/10.1021/acs.energyfuels.7b01387.
(62) Kang, W.; Jing, G.; Zhang, H.; Li, M.; Wu, Z. Influence of Demulsifier on Interfacial Film between Oil and Water. *Colloids and Surfaces A: Physicochemical and Engineering Aspects* **2006**, *272* (1–2), 27–31. https://doi.org/10.1016/j.colsurfa.2005.07.004.
(63) Liu, J.; Zhao, Y.; Ren, S. Molecular Dynamics Simulation of Self-Aggregation of Asphaltenes at an Oil/Water Interface: Formation and Destruction of the Asphaltene Protective Film. *Energy Fuels* **2015**, *29* (2), 1233–1242. https://doi.org/10.1021/ef5019737.

TOC Graphic

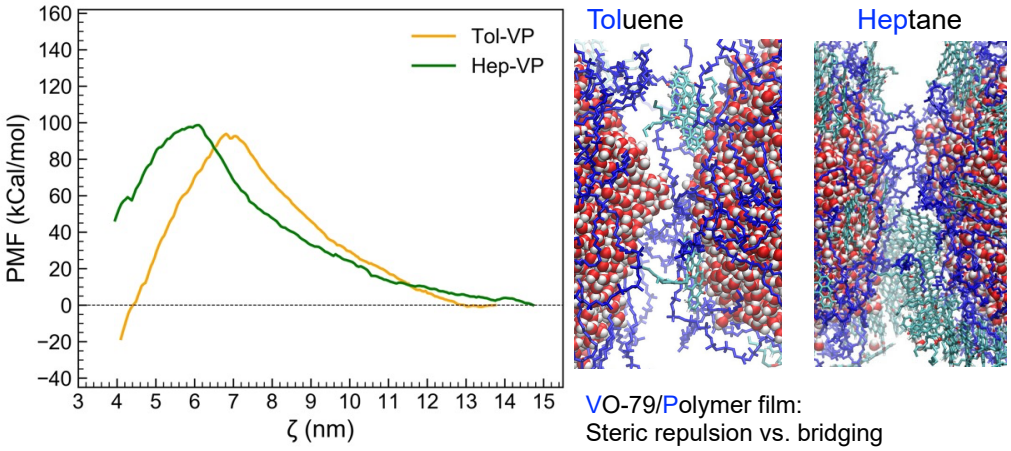

VO-79/Polymer film:
Steric repulsion vs. bridging